IOP Conf. Series: Materials Science and Engineering **382** (2018) 042022 doi:10.1088/1757-899X/382/4/042022

Behaviours of Spatial Beam-to-Corner Column Joint with T-stub under cyclic loading

Xin BU [1,2], Qian GU [1] and Xinwu WANG [2]

[1] School of Civil Engineering and Architecture, Wuhan University of Technology, Wuhan 430000, Hubei China

[2] Department of Civil Engineering, Luoyang Institute of Science and Technology, Luoyang 471023, Henan China

carville@163.com

Abstract. The prediction of the behaviour of Spatial joint and plane joint relied on experimental and numerical tests that provide accurate information for the characterization of the beam to Column connection with T-stub. The corner column connections of steel frame as the research object and there are one spatial T-stub connection specimen and one plane T-stub connection specimen. Spatial cyclic load of quasi-static tests and finite element analysis were carried out, of which load was applied to the column. According to the results of quasi-static tests and finite element calculations, difference of joints' rotational stiffness, hysteretic property, ductility coefficient and energy dissipation characteristics were analysed. It is verified that the mechanical characteristics of spatial semi-rigid joint under spatial load are different from plane semi-rigid joint under plane load.

1. Introduction

A large number of welded beam-to-column joints in steel moment resisting frames failed in a brittle manner during the Northridge and Kobe earthquakes because of premature fracture of the welds [1, 2]. The main reasons for the extensive failure include possible weld deficiencies and more importantly, lack of understanding of such joints under earthquakes [3]. The critical lessons drawn from these major earthquakes led to intensive research investigations into the strategies of improving the ductility of welded beam-to-column joints against seismic action. Presently, to solve the beam–column connection problem of steel-frame structures, domestic and foreign experts have performed a series of experimental studies on the anti-seismic properties of related typical semi-rigid plane beam–column joints. Existing experimental studies on semi-rigid joints mainly focused on the plane joint [4-9]. However, in the practical framework structure, the joints could be divided into interior column connections, side column connections, and corner column connections according to the spatial position of the joints. Under seismic action, the three types of joints possess characteristics such as spatial stress, and the frame joints bearing the bending moment, torque, shear force, and axial force that are transferred from the beams and columns in multiple directions. Under the joint action of these internal forces, the mechanical properties and failure mechanism of the joints become very complicated [10, 11]. Therefore, research on the seismic behaviour of the spatial joints under space stress is of considerable significance for guiding the seismic design of a steel-frame structure system.

Content from this work may be used under the terms of the Creative Commons Attribution 3.0 licence. Any further distribution of this work must maintain attribution to the author(s) and the title of the work, journal citation and DOI.
Published under licence by IOP Publishing Ltd

2. Design of the test specimens

Beam to column connection with T stub is one of the typically semi-rigid beam-column connections, and they feature in large rotational stiffness and bearing capacity [13, 14]. As shown in Figure1, pseudo static test was carried out on the spatial corner joint in spatial frame with T stub. Meanwhile, to study the different characteristics between the plane joint and the spatial joint, pseudo static test was also carried out on the plane joint, See Figure2. The models for all the test specimens were made at a scale of 1:1. The beams of the spatial joint were connected to the column with T stubs and high-strength bolts. In the plane of the joint's major axis, the beam was connected to the column flange and in the plane of the minor axis, the beams were connected to the column web. Columns and beams in the test were made from WH300×300×10×15 and NH350×175×7×11 hot rolled H sections. The T stubs were T270×200×9×14. See Table1 for detailed information about the joints. All the test specimens at the joints were connected with high strength friction bolts (Grade 10.9, M22). The beams and columns were fixed in accordance with the Code for Acceptance of Construction Quality of Steel Structures (GB50205-2001).

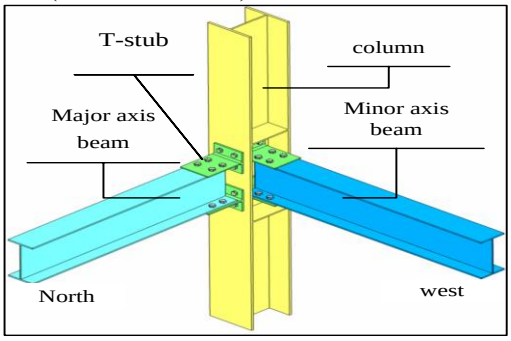

Figure 1. Spatial joint specimen.

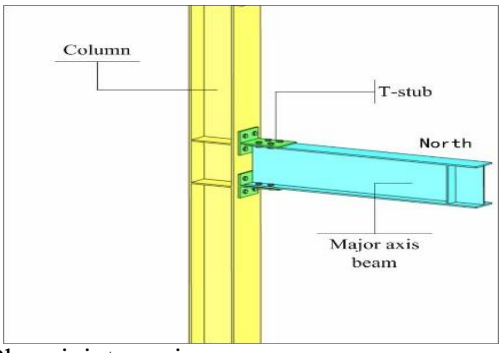

Figure 2. Plane joint specimen.

Table 1. Parameters of the test Specimens

Joint ID	Length of column (mm)	Length of the beam at the major axis (mm)	Length of the beam at the minor axis (mm)	Bolt Spec.	Bolt Qty.
JDA	3000	1800	—	M22	16
JDB	3000	1800	1900	M22	40

Table 2. Mechanical performances of the steel used for the test

Steel category	Test items			
	f_y(MPa)	f_u (MPa)	A (%)	E(GPa)
Columns' web and flange average value of tensile strength	271	457	36	209
Beam s' web and flange average value of tensile strength	270	460	28.5	209
T stubs' web and flange average value of tensile strength	260	456	36.5	207

All beams, columns, and T stubs were made from Q235B steel from the same lot. The steel has been made into test specimens according to Metallic Material Room Temperature Tension Test Methods (GB/T288.1-2010) for the strain–stress curve uniaxial tension tests. See Table2 for the outcome of the steel's mechanical performance tests.

3. Test devices

At present time, in quasi-static test of beam-to-column joints, most of which adopt the method of beam end loading mode and less column loading mode, Although the beam end loading method can make the stress state of the joint basically coincide with the actual stress state, but it neglects the P-Δ second-order effect. On the basis of the mechanical characteristics of beam to column joints in frame (Figure3), two pairs of horizontal actuators were separately placed in the joints' major axis plane and

minor axis plane. The two planes were orthogonal to each other. Each pair of actuators was fixed to a L-shaped reaction wall, and horizontal loads were applied to both ends of the column. A vertical actuator fixed with a reaction frame was arranged at the top of the column so that axial pressure can be applied on column. The vertical actuator can horizontally move with the end in both directions. The above five actuators were controlled by an electro hydraulic servo testing system. The north–south direction was the joint's major axis plane, and the east–west direction was the minor axis plane. At the foot of the column, a hinged support that was able to move in all directions was used to achieve slide displacement due to orthogonal loads in two directions. Hinged supports that were able to follow the movement of the beam ends were arranged at the beam ends in the east (E), west (W), and north (N) directions. The supports were hinged in the plane of the applied loads and moved with the ends out of the planes of loads. Meanwhile, pressure sensors were placed at the upper and lower ends of each beam to measure the reaction force of the supports at the beam ends. Each of the beam-end supports was placed on a lattice truss that has large stiffness. See Figure 4 for the test sites of the spatial joint specimen and the test sites of the plane joint specimen is shown in Figure5, and test load step curve is shown in Figure6 [12].

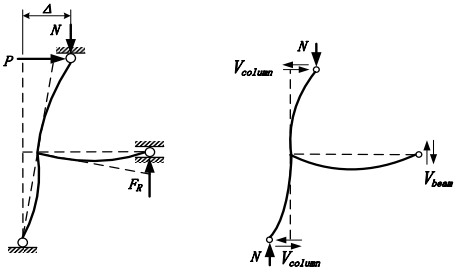

Figure 3. Mechanical model of the beam–column joint.

Figure 4. Spatial joint test site.

Figure 5. Plane joint test site.

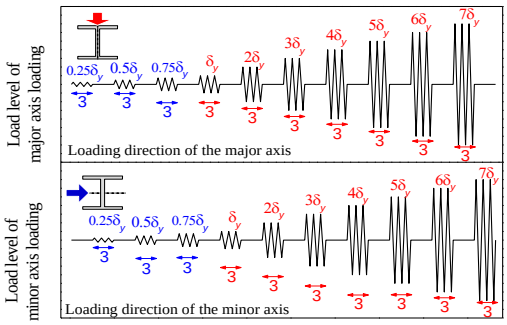

Figure 6. Bidirectional load step curve.

4. Finite element model

In order to analyse and understand the behaviours of beam-to-column joints under cyclic load, the Finite Element Method software ABAQUS was used. A three-dimensional (3-D) finite element model of the spatial corner joint and plane joint was developed on standard static analysis. Figure 7 shows the meshing established for plane joint model and spatial joint model was shown in Figure 8. In order to obtain some simplification on the modelling, only fine mesh was defined when closer to the contact part of the model. 8-node linear brick elements with reduced integration C3D8R were considered for most components. A series of contact interactions were defined between the connector and the column/beam, and between the bolts and the connected members. Surface-to-surface contacts with finite sliding were employed for all the contacting pairs, where “Hard” contact was assumed for the normal contacting behaviour and a friction coefficient of 0.4 was assumed for the tangential behaviour, as recommended by the Chinese Standard. It is also noted that the diameter of the bolt shank was taken as the same as the bolt hole (i.e. no bolt hole clearance) to enable initial contact and thus to

allow good numerical convergence. Before the cyclic loading, the 190kN pre-tightening force was applied to each bolt.

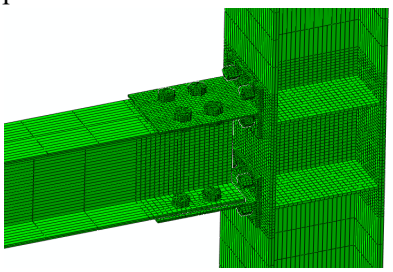

Figure 7. Finite element model of plane joint.

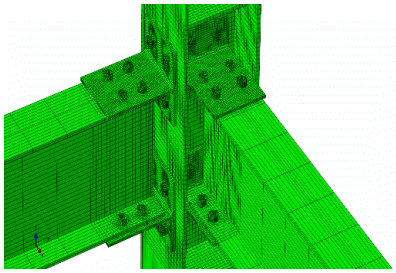

Figure 8. Finite element model of spatial joint.

5. Test results and finite element analysis

5.1. Yielding behaviors and failure modes

According to compare experimental and numerical results, whether plane joint or spatial joint the yielding locations tended to be concentrated on the T-stubs. For the test specimen at the plane joint (JDA) under the cyclic load, the upper T stub and lower T stub in the plane joint (JDA) became quite plastic and deformed, When the connection under the maximum load, T stub's flange was separated from the column's flange and created a gap between column's flange and T stub's flange(Figure9& Figure10).The spatial joint (JDB) in 3D frame had the feature of destruction in the plane of the major axis also occurred at the T stubs, and the cracking is developed gradually under the cyclic load. The feature of destruction in the plane of the minor axis occurred at the column's web, which has a large plastic deformation. The main reason was that beam was connected to the column's web with T stubs, in the direction of the minor axis the T stub's flange was thicker than the column's web, therefore, when the plane of the minor axis was under cyclic load, the T stubs on one side of the column's web caused the column's web to deform out-of-plane due to the pull and press effects. Destruction of the spatial joint showed in Figure11, and finite element analysis result is shown in Figure12.

Figure 9. Fracture failures of plane joint.

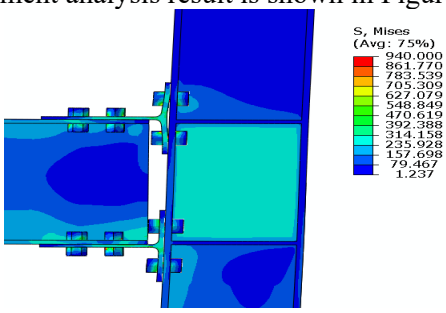

Figure 10. Fracture failures of plane joint with FEA.

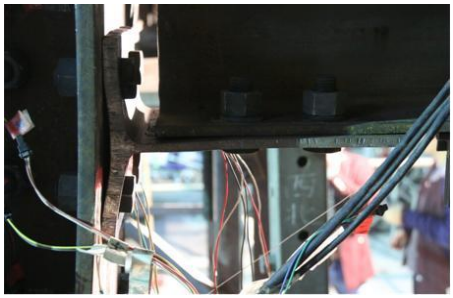

Figure 11. Fracture failures of spatial joint.

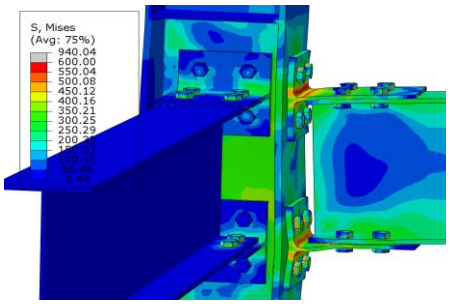

Figure 12. Fracture failures of spatial joint with FEA.

5.2. Hysteresis curve and Skeleton curve analysis

The *M-θ* hysteresis curves for all joints in this test and finite element analysis are shown in Figure13. The skeleton curve for each joint specimen in each direction is illustrated in Figure14. The hysteresis curve of each joint specimen shows a fusiform shape without pinching, it is indicated that the energy dissipation characteristic of each joint is better. The skeleton curves of plane joint specimen (JDA), in the major axis of the plane showed significant decline, mainly due to the T stub connector under cyclic loading has a plastic deformation. Due to the minor axis plane bearing internal forces, the yield state moment capacity of the major axis plane of the spatial joint is 21.4% lower than that of the plane joint, and also ultimate state moment capacity decreased by 6.1%.The results show that the deformation about column web being out of minor axis plane has a greater influence on the yield-bending moment capacity of the major axis plane, yet the ultimate state moment capacity is less affected. Result of the finite element analysis and the result of the test are coincide well.

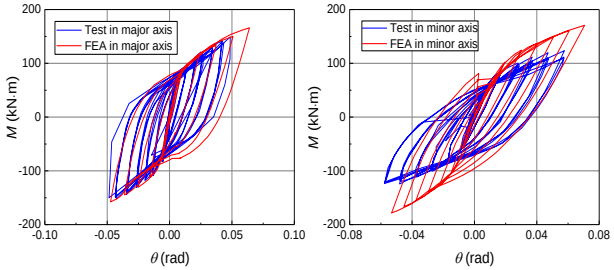

Figure 13. Hysteresis curves of the JDB.

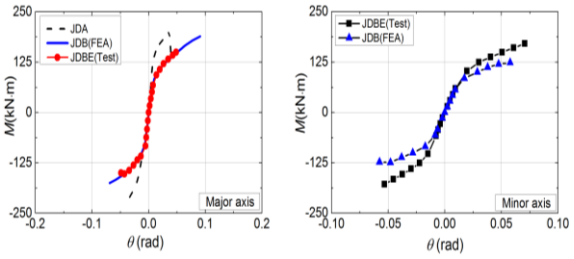

Figure 14. Skeleton curves of JDA&JDB.

Table 3. Test results and FEA results

Joint No.	Direction	Loading Direction	Yield state (Test)	Ultimate state (Test)	Yield state(FEA)	Ultimate state (FEA)
			M_y (kN· m)	M_u (kN· m)	M_y (kN· m)	M_u (kN· m)
JDA	North	Positive	110.79	201.03	53.23	163.27
		Negative	-80.79	-120.21	-79.48	-163.75
JDB	North	Positive	67.4	149.17	67.8	188.74
		Negative	-83.22	-152.48	-65.58	-175.29
	West	Positive	42.21	123.51	44.38	170.71
		Negative	-42.22	-122.81	-43.22	-178.25

5.3. Analysis of the degradation of rotational stiffness

Rotational stiffness of the joint before the yield load corresponded to the moment-rotation tangent stiffness. After entering the plastic state, the bending moment and the rotation angle showed nonlinear properties. For the purpose of convenience, secant stiffness was commonly used to represent the rotational stiffness. Hence, the rotational stiffness of the joint (Eq. 1) was calculated as follows:

$$K_i = \frac{|+M_i|+|-M_i|}{|+\theta_i|+|-\theta_i|} \tag{1}$$

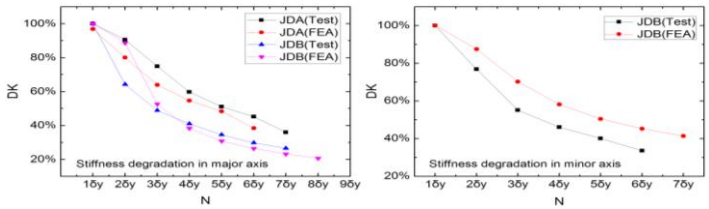

Figure 15. Rotational stiffness degradation curves.

M_i is the peak value of the moment bearing capacity under certain level of loads, and θ_i is the rotation that corresponds to the peak value of the moment bearing capacity under certain levels of loads. The initial rotational stiffness at the north side of the plane joint (JDA) is 14326.52 kN·m/rad and the initial rotational stiffness at the north side of the spatial joint specimen (JDB) is 8137.67 kN·m/rad, the initial rotational stiffness of the major axis is about 43.2% lower than that of the plane joint (JDA).The rotational stiffness degradation of the joints degenerated with the increasing load is shown in Figure 15, in which DK represents the stiffness degradation rate and N represents the load level. With respect to the semi-rigid joints, the initial rotational stiffness degradation of the spatial joint was faster than that of the plane joint. When the plane joint was destructed, the rotational stiffness degraded to lower than 36.33% of the initial value. In the state of failure, spatial joint specimen's stiffness of the major axis degenerated to 27.56% of the initial stiffness, and the west side of the minor axis degenerated to 32.43% of the initial stiffness. The above analysis shows that the spatial joint with smaller initial rotational stiffness under the action of a cyclic reciprocating load had faster stiffness degradation. Minor axis plane has great influence on the initial rotational stiffness of the major axis.

5.4. Ductility coefficient of the rotation angle

The ratio of the ultimate rotation angle θ_u to the yield rotation angle θ_y was used to describe the ductility coefficient. The ductility coefficients of the test joints in all directions are shown in Table 4 and were expressed as the average of the major axis and minor axis. The ductile coefficient of connection is the average value in the positive and negative directions of the major and minor axis. When the loads of a spatial joint in the minor axis plane are taken into consideration, the ductility of the spatial joint in the major axis plane increased. According to the table4, the ductile coefficient of the spatial joint in the major axis plane was 80.3% higher than that of the plane joint. From the above analysis, it can be concluded that the ductile coefficient of the spatial joint was higher than that of the plane joint.

Table 4 Ductility factor of specimens

Joint ID	Major axis		Minor axis	
	TEST	FEA	TEST	FEA
JDA	4.06	4.86	—	—
JDB	7.32	7.74	8.73	7.37

5.5. Energy dissipation capacity

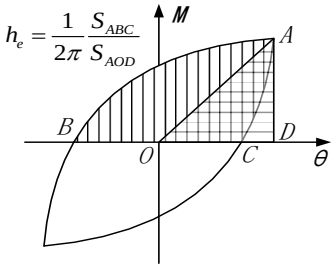

Figure16. Equivalent viscous damping coefficient calculation diagram.

Table 5 Equivalent viscous damp coefficient

Joint ID	Major axis		Minor axis	
	TEST	FEA	TEST	FEA
JDA	0.286	0.294	—	—
JDB	0.241	0.298	0.222	0.232

For the joints' energy dissipation capacities, the equivalent viscous damping coefficient, he, is usually used to evaluate the amount of energy absorbed by a test Specimen under cyclic loading. The calculation can be carried out according to Figure16, while calculation results are shown in Table 5. As observed from Table 5, the equivalent viscous damping coefficient of a joint is the average value in the positive and negative directions of the major and minor axes. When the loads of the spatial joint in the minor axis plane were taken into consideration, the equivalent viscous damping coefficient of the spatial joint (JDB) was relatively lower than that of the plane joint (JDA), On the basis of the above analyses, when the impact of loads on the joint in the minor axis plane and the locations of the joints in the frame are taken into consideration, they have varying degrees of influence on the joints' energy dissipation characteristics.

6. Summary

The following three conclusions are obtained through analysis

(1) The moment capacity of the spatial joint is lower than that of the plane joint, and the same relative about the rotational stiffness of the spatial joint is lower than that of the plane joint, the coefficient of ductility of spatial joint is also different from that of plane joint.

(2) The plastic hinge of the connection mainly appears at the junction of the web and the flange of the T stub, where the plastic strain develops fastest and most obviously, so T stub is a key factor affecting joint's mechanical properties.

(3) A preliminary numerical study was carried out to further investigate the behaviour of the proposed joints, where it was found that the numerical results agree well with the test results. I Based on the test and numerical results, and this method was put forth for normal design of such connections.

References

[1] Mahin S A 1998 Lessons from damage to steel buildings during the Northridge earthquake *Eng.Struct* **20** 261-270.
[2] Nakashima M K, Inoue M T 1998 Classification of damage to steel buildings observed in the 1995 Hyogoken-Nanbu earthquake *Eng. Struct* 20 271-281.
[3] Barsom J M Pellegrino J V 2002 Failure analysis of welded steel moment-resisting frame connections *J. Mater. Civ. Eng* **14** 24-34.
[4] Kim T, Whittaker A S and Gilani A 2002 Experimental evaluation of plate-reinforced steel moment-resisting connections *J. Struct. Eng* **128** 483-491.
[5] Lee C, Jung J 2003 Cyclic seismic testing of steel moment connections reinforced with welded straight haunch *Eng. Struct* **25** 1743-1753.
[6] Tanaka N 2003 Evaluation of maximum strength and optimum haunch length of steel beam-end with horizontal haunch *Eng. Struct* **25** 229-239.
[7] Mirghaderi S R, Torabian S and Imanpour A 2010 Seismic performance of the accordion web RBS connection *J. Constr. Steel Res* **66** 277-288.
[8] Wilkinson S, Hurdman G and Crowther A 2006 A moment resisting connection for earthquake resistant structures *J. Constr. Steel Res* **62** 295-302.
[9] Kim Y, Ryu H 2009 Seismic performance of steel structures with slit dampers *Eng. Struct***31** 1997-2008.
[10] Fan J S, Zhou H, Nie J 2014 Experimental study on seismic performance of three-dimensional composite beam-to-column joints *J. China Civil Eng* **04** 47-55.
[11] Fan J S, Zhou H, Nie J 2011 Experimental study on seismic performance of three-dimensional composite beam-to-column joints *J. Building Struct* **12** 37-45.
[12] FEMA-461 2007 Interim testing protocols for determining the seismic performance characteristics of structural and non-structural components.